Biochemical and Biophysical Research Communications 452 (2014) 436–442

Contents lists available at ScienceDirect

Biochemical and Biophysical Research Communications

journal homepage: www.elsevier.com/locate/ybbrc

Solution structure of telomere binding domain of AtTRB2 derived from *Arabidopsis thaliana*

Ji-Hye Yun [a,1], Won Kyung Lee [b,1], Heeyoun Kim [a], Eunhee Kim [c], Chaejoon Cheong [c], Myeon Haeng Cho [b,*], Weontae Lee [a,*]

[a] Department of Biochemistry, College of Life Science and Biotechnology, Yonsei University, Seoul 120-749, Republic of Korea
[b] Department of Systems Biology, College of Life Science and Biotechnology, Yonsei University, Seoul 120-749, Republic of Korea
[c] Magnetic Resonance Team, Korea Basic Science Institute (KBSI), Ochang, Chungbuk 363-883, Republic of Korea

ARTICLE INFO

Article history:
Received 16 August 2014
Available online 27 August 2014

Keywords:
Arabidopsis thaliana telomere repeat binding factor 2 (AtTRB2)
NMR spectroscopy
Solution structure
Telomere-associated protein
Single-Myb-Histone (SMH)

ABSTRACT

Telomere homeostasis is regulated by telomere-associated proteins, and the Myb domain is well conserved for telomere binding. AtTRB2 is a member of the SMH (Single-Myb-Histone)-like family in *Arabidopsis thaliana*, having an N-terminal Myb domain, which is responsible for DNA binding. The Myb domain of AtTRB2 contains three α-helices and loops for DNA binding, which is unusual given that other plant telomere-binding proteins have an additional fourth helix that is essential for DNA binding. To understand the structural role for telomeric DNA binding of AtTRB2, we determined the solution structure of the Myb domain of AtTRB2 ($AtTRB2_{1-64}$) using nuclear magnetic resonance (NMR) spectroscopy. In addition, the inter-molecular interaction between $AtTRB2_{1-64}$ and telomeric DNA has been characterized by the electrophoretic mobility shift assay (EMSA) and NMR titration analyses for both plant (TTTAGGG)n and human (TTAGGG)n telomere sequences. Data revealed that Trp28, Arg29, and Val47 residues located in Helix 2 and Helix 3 are crucial for DNA binding, which are well conserved among other plant telomere binding proteins. We concluded that although AtTRB2 is devoid of the additional fourth helix in the Myb-extension domain, it is able to bind to plant telomeric repeat sequences as well as human telomeric repeat sequences.

1. Introduction

Most eukaryotic chromosomal DNA molecules have particular nucleotide sequences called telomeres at the physical ends of their linear chromosomes [1]. Telomeres consist of multiple copies of repetitive DNA, which are tandem arranged and are classified non-coding DNA. In plant telomeres, the repeated unit is the seven nucleotide sequence TTTAGGG [2] and in human telomeres, it is the six nucleotide sequence TTAGGG [3]. On account of the telomeres, the eukaryotic genome is protected from being eroded through each round of DNA replication and maintained its integrity and stability in stem cells [4], reproductive cells [5], and cancer cells [6]. In addition, telomeres prevent chromosomal end-to-end fusion in homologous recombination and non-homologous end joining as well as help chromosomes to attach to the nuclear envelope [7].

During the entire process of the cell division cycle, the preservation of the telomeric repeated unit requires a special mechanism, because of the end replication problem in which the final daughter DNA strand that results from lagging strand synthesis through a backstitching mechanism would be shortened at each cell division [8]. In this special mechanism, telomerase is indispensable. Telomerase is a telomere-specific ribonucleoprotein reverse transcriptase and adds multiple telomeric repeats to its 3′ end by using its own associated RNA, which contains a ribonucleotide sequence that serves as a template for the addition of deoxyribonucleotides to the ends of the telomere segments [9]. Telomere homeostasis is regulated by telomere-associated proteins. hTRF1 (telomeric repeat-binding factors 1), hTRF2 (telomeric repeat-binding factors 2) and POT1 (protection of telomeres) in human and AtTBP1, AtTRB1 and POT1 in plant are well known telomere binding proteins and those have the Myb domain or homeodomain, which has the general features of the telomeric repeat double-stranded DNA binding protein family, binds to DNA for regulating gene expression, coordinating the transcription of developmental genes, and switching them on or off [10–13]. The Myb domain refers to a telo-box located at the C-termini of telomere-binding proteins found in

* Corresponding authors. Fax: +82 2 363 2706.
E-mail address: wlee@spin.yonsei.ac.kr (W. Lee).
[1] Co-first author.

http://dx.doi.org/10.1016/j.bbrc.2014.08.095
0006-291X/

both animals and plants (hTRF1, hTRF2, Rap1, RTBP1, NgTRF1, AtTBP1, and AtTRP2) [14–18]. Other groups of telomere binding proteins with Myb domain at their N-termini have been found only in plant proteins [14,18–20]. Single Myb histone (SMH) family proteins have three domains; the N-terminal Myb domain with three α-helical bundles, the globular GH1/GH5 domain in the middle region, and the coiled-coil domain near the C-terminus [20]. In *Arabidopsis thaliana*, AtTRB2 (AGI ID: At5g67580) belongs to this family and binds to the double-stranded plant telomeric DNA. The Myb-like domain of AtTRB2 ($AtTRB2_{1-64}$) is homologous to that of other telomere binding proteins in both plants and animals. Unusual, it is devoid of the additional fourth helix in the Myb-extension domain unlike common telomere binding proteins in plant. Therefore, it will be very helpful to know the three-dimensional structure and DNA binding mode of $AtTRB2_{1-64}$ to understand the molecular function of the SMH family protein. Here, we report the NMR structure and DNA binding mode of $AtTRB2_{1-64}$ by EMSA analysis and NMR spectroscopy.

2. Materials and methods

2.1. EMSA assay

To determine the molecular interaction between telomeric DNA and AtTRB2, supershift construct of AtTRB2 Myb proteins ($AtTRB2_{1-60}$, $AtTRB2_{1-64}$, $AtTRB2_{1-65}$, $AtTRB2_{1-77}$, $AtTRB2_{1-97}$) including glutathione S-transferase (GST) tag were clone using the pGEX-5X-1 vector (Amersham Pharmacia Biotech, USA) and expressed in *Escherichia coli* BL21 (DE3)/RIL cells (Stratagene), and purified using GSTrap™ column. The concentration of protein sample was determined by the Bradford method and final samples were stored at −80 °C. Purity of protein samples was analyzed by sodium dodecyl sulfate polyacrylamide gel electrophoresis (SDS–PAGE). The EMSA method was executed as previously reported [21,22]. Both plant and human types of telomeric DNA probes with competitors were designed and labeled using [γ-^{32}P] Adenosine triphosphate (ATP), and 0.5 μg of poly (dI-dC) were used to prevent non-specific DNA binding. For competition experiments, competitors were pre-incubated with a reaction mixture before the reaction with the radiolabeled probe. An Image Gauge Version 2.53 (Fuji Photofilm) was utilized for the quantification of the binding activity.

2.2. Construct design, protein expression and purification

The $AtTRB2_{1-64}$ was cloned into the pET15b vector (Novagen) including His-tag and a chaperon-like functional peptide (GRIFLQD). The specific cleavage sequence of the tobacco etch virus (TEV) protease, ENLYFQG, was inserted in front of the $AtTRB2_{1-64}$. Protein expression was induced in *E. coli* BL21 (DE3) cells (Novagen) with 1 mM isopropyl-1-thio-β-D-thiogalactoside (IPTG) in optical density values of 0.6 at 600 nm. After 12 h of incubation, cultured cells were harvested and the cell pellet was broken up in the lysis buffer, 10 mM Na_2HPO_4, 2 mM KH_2PO_4 (pH 7.4), 2.7 mM KCl, 137 mM NaCl, 1 mM EDTA, using sonication. After centrifugation at 15,000 rpm, at 4 °C for 25 min, the collected inclusion bodies were solubilized in a PBS buffer (pH 7.4) including 6 M guanidine-HCl at room temperature for 5 h. After resolubilization, the insoluble pellet was removed using centrifugation, and soluble fraction was used for nickel affinity chromatography work. For the gradient refolding of target proteins, we followed the efficient on-column refolding scheme in AKTA™ prime with HiTrap™ (GE Life Sciences). Refolded $AtTRB2_{1-64}$ was eluted in 10 mM HEPES (pH 7.0), 100 mM NaCl and 500 mM imidazole. The His-tag was removed through the TEV protease, and pure $AtTRB2_{1-64}$

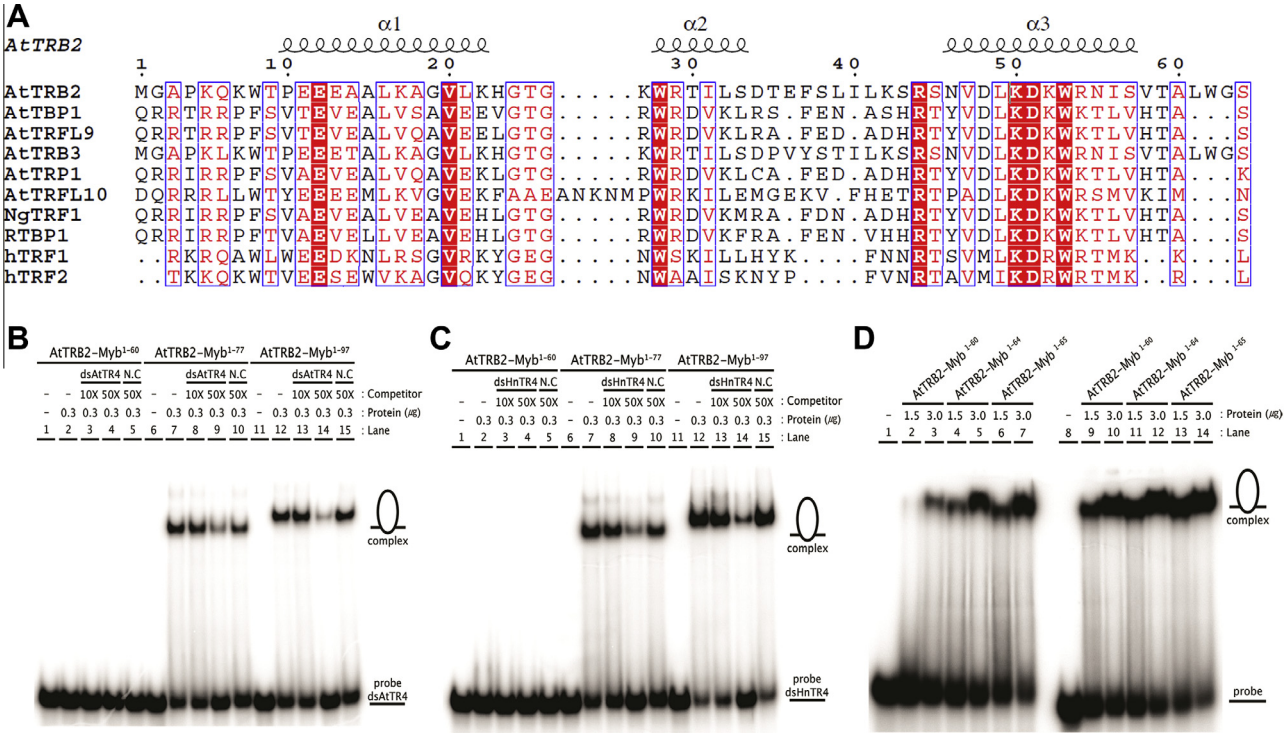

Fig. 1. Sequence alignment and EMSA assay of $AtTRB2_{1-64}$ for DNA binding. (A) Multiple sequence alignment between $AtTRB2_{1-64}$ and corresponded regions of other telomeric DNA-binding proteins suggested that whether in plant or human telomere binding proteins, the Myb domain is highly conserved. Sequence alignment was achieved by T-COFFEE and it was rendered by ESPript. (B, C) Competitive EMSA assay between the $AtTRB2_{1-64}$ and plant-type telomeric DNA (dsAtTR4) (B) and human-type telomeric DNA (dsHnTR4) (C). Three different truncated Myb constructs of AtTRB2 (GST-$AtTRB2_{1-60}$, GST-$AtTRB2_{1-77}$, and GST-$AtTRB2_{1-97}$) were used in the same concentration (0.3 μg) and unlabeled plant-type telomeric DNA was gradually added as a competitor. (D) Minimized constructs of the Myb-domain of AtTRB2 (GST-$AtTRB2_{1-60}$, GST-$AtTRB2_{1-64}$, and GST-$AtTRB2_{1-65}$) were used (3 μg). From land 2 to 7, it showed the protein/plant DNA complex and from land 9 to 14, it showed the protein/human DNA complex. Land 1 and 8 were negative controls, which did not add a protein sample.

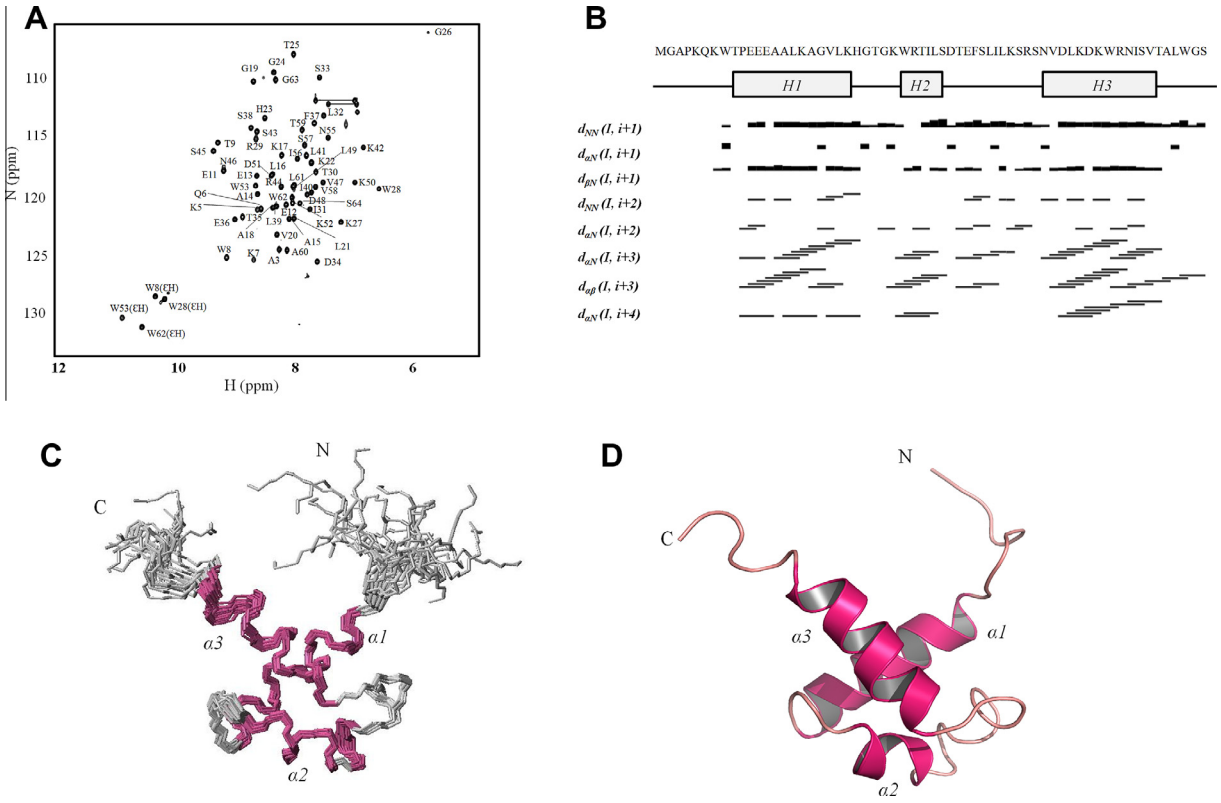

Fig. 2. Solution structures of AtTRB2$_{1-64}$. (A) $^{1}H-^{15}N$ HSQC spectrum of uniformly $^{13}C/^{15}N$-labeled AtTRB2$_{1-64}$. Each peak corresponds to an amide N and H of each amino acid residue. The spectrum was collected at pH 7.0 and 298 K on a Bruker DRX 500 MHz cryoprobe NMR spectrometer. (B) Secondary structure of AtTRB2$_{1-64}$ is shown by NOE connectivities, represented by the line thickness classifying NOE intensity which extracted from ^{15}N-, ^{13}C-edited NOESY spectra. (C) Main-chain atoms of the final 20 lowest energy calculated structures. The α-helical regions (residue 10–58) were superimposed. (D) Ribbon diagram of the AtTRB2$_{1-64}$ structure. It consists of three α-helices (colored by hot-pink). (For interpretation of the references to color in this figure legend, the reader is referred to the web version of this article.)

Table 1
Structural statistics for the final calculated structures of AtTRB2$_{1-64}$.

	DNA binding domain of AtTRB2 (residue numbers: 1–64)
NOE distance constraints	
All	1000
Short range ($\|i-j\| \leqslant 1$)	597
Intraresidue NOEs ($\|i-j\| < 1$)	332
Sequential NOEs ($\|i-j\| = 1$)	265
Medium range ($1 < \|i-j\| < 5$)	270
Long range ($\|i-j\| \leqslant 5$)	133
Hydrogen bond constraints	42
Dihedral constraints	
All	45
Φ	22
Ψ	23
Mean CYANA target function (Å^2)	0.17 ± 0.06
Number of restraint violations	
Total number of distance violations >0.5 Å	0
Total number of hydrogen bond violation >0.5 Å	0
Total number of dihedral angle violations >5	0
Mean RMS deviations from the average coordinate (Å)[a]	
Backbone atoms (N, C_α, C′, O)	0.41 ± 0.08
Heavy atoms	1.03 ± 0.13
Ramachandran plot (%)[b]	
Residues in most favored regions	83.5
Residues in additional allowed regions	16.4
Residues in generously allowed regions	0.1
Residues in disallowed regions	0.0

[a] Calculation of RMSD was used by residues 510–609.
[b] Ramachandran plot was calculated using the PROCHECK program.

was isolated by size exclusion gel chromatography with HiLoadSuperdex 75 prep grade column (Pharmacia). For the preparation of the NMR samples, M9 minimal media and isotopes (^{13}C-glucose and $^{15}NH_4Cl$) were used during the cell culture. All NMR samples were prepared in 10 mM HEPES (pH 7.0), 100 mM NaCl with 0.01% NaN_3 including 90% H_2O/10% D_2O.

2.3. NMR spectroscopy and structure determination

All NMR spectra were obtained by triple-resonance experiments at 298 K on a Bruker DRX 500 MHz spectrometer with triple axis gradient coils equipped with a 5 mm triple-resonance cryoprobe. Sequential backbone chemical shifts were completely assigned using $^{1}H-^{15}N$ heteronuclear single quantum coherence, HNCACB, CBCACONH, HNCA, and HNCO [23–26]. Side-chain chemical shift assignments were executed by HBHACONH, HCCCONH, and HCCH-TOCSY. Inter and intra residual NOEs were observed in three dimensional ^{15}N-edited and ^{13}C-edited NOESY (τ_m = 600 ms) [27,28]. All NMR data were processed through the NMRPipe/NMRDraw software package [29] and resonance peaks were analyzed using Sparky 3.113 software [30]. Torsion angle (Ψ, Φ) from TALOS analysis [31] and hydrogen bonds were used for structural restraints in the CYANA program [32]. The initial 100 conformers were computed using 10,000 torsion angle dynamics steps, and 20 energy-minimized structures were selected. Final structures were analyzed with PROCHECK [33] and visualized using MOLMOL [34] and PyMOL programs [35]. For the NMR titration, both plant (5′-(TTTAGGGTTTAGGG)-3′) and human (5′-(TTAGGGTTAGGG)-3′) types of telomeric DNA were used. The $^{1}H-^{15}N$ HSQC spectra were

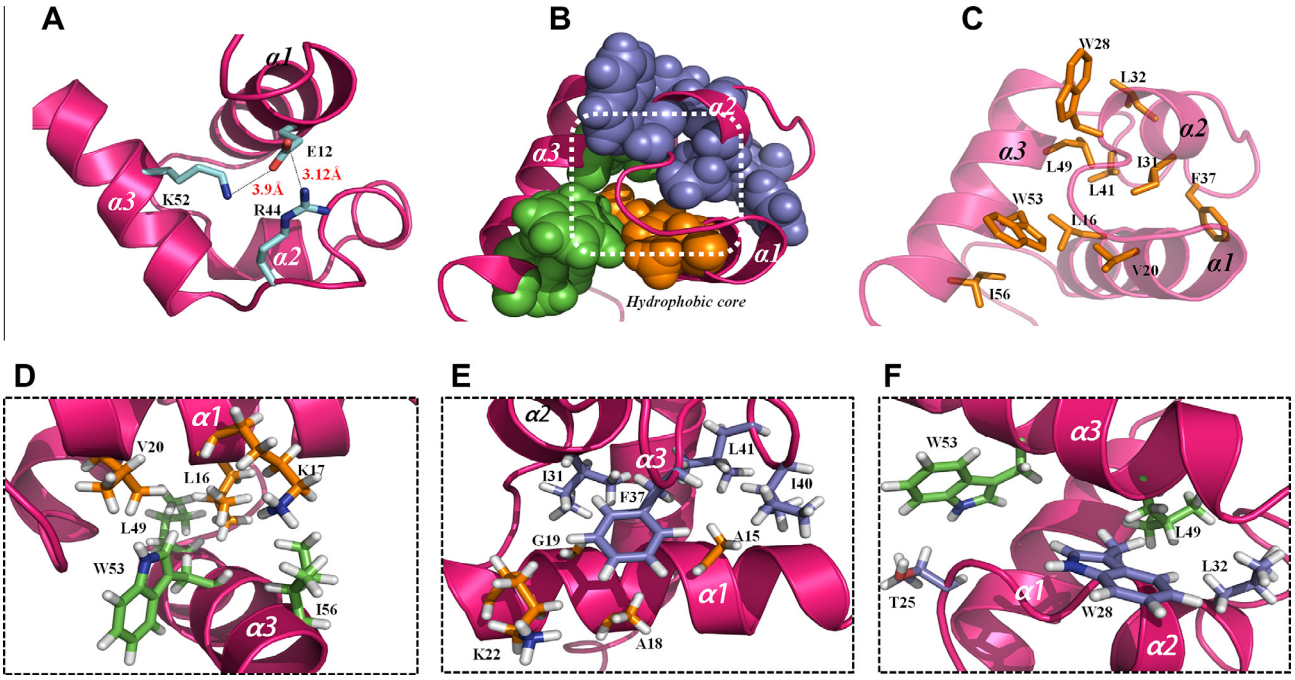

Fig. 3. Structural overviews of AtTRB2$_{1-64}$. (A) Dashed lines indicate the salt bridges. Two salt bridges contributed to the stability of the overall folding structure. Red and blue atoms mean oxygen and nitrogen, respectively. (B, C) Hydrophobic core patch is formed by the side-chain connectivity of hydrophobic residues located in three helices. It is represented by spheres (B) and stick (C) model. The overall structure is maintained by these hydrophobic interactions. All hydrogen atoms do not present. (D–F) Detail views of hydrophobic side-chain connectivity between α1 and α3 (D), α1 and α1–α2 loop/α2 (E) and α2 and α3 (F) region. Hydrophobic residues located in α1, α2 and α3 are colored by orange, violet and green, respectively. (For interpretation of the references to color in this figure legend, the reader is referred to the web version of this article.)

recorded for different molar ratios of DNA: protein of 1:0, 1:0.25, 1:0.5, 1:0.75 and 1:1, respectively.

3. Results and discussion

3.1. EMSA assay for characterization of DNA binding domain of AtTRB2

Data from multiple sequence alignments among telomere binding proteins suggest that the Myb domains of both plant and human telomere binding proteins are highly conserved (Fig. 1A). To determine the DNA binding domain of AtTRB2, three AtTRB2 domains (GST-AtTRB2$_{1-60}$, GST-AtTRB2$_{1-77}$, and GST-AtTRB2$_{1-97}$, GST-AtTRB2$_{1-64}$, and GST-AtTRB2$_{1-65}$) were used. Both plant-type and human-type telomeric repeat sequences were used as a probe for the competitive EMSA assay method. Both AtTRB2$_{1-77}$ and AtTRB2$_{1-97}$ were completely shifted for plant telomeric DNA, and those intensities were gradually decreased by the addition of a competitor (Fig. 1B). These results were also observed for human telomeric DNA (Fig. 1C). Together with, AtTRB2$_{1-64}$ is a minimum length of the Myb domain, which binds to both plant and human telomeric DNA sequences (Fig. 1D).

3.2. NMR resonance assignments and structure calculations

The AtTRB2$_{1-64}$ protein was promptly confirmed through the ^{1}H–^{15}N HSQC experiment as to whether its fold could be settled or not. And the resonance peaks in this spectrum are well-spread out indicating a well-defined tertiary structure (Fig. 2A). To calculate the three-dimensional structure, 1000 upper distance limits [332 intra-residual, 265 sequential, 270 medium-range ($2 \leqslant |i-j| < 5$), and 133 long-range ($|i-j| \geqslant 5$)] derived from NOESY cross-peak intensities, 45 dihedral angle constraints [22 for the angle of rotation about the bond between the amide nitrogen and the alpha carbon (Φ), 23 for the angle of rotation about the bond between the alpha carbon and the carbonyl carbon (Ψ)] and 42 backbone hydrogen bond constraints were applied. None of the final 20 energy-minimized structures detected violations about distance constraints or van der Waals constraints of greater than 0.2 Å or angle restraints of greater than 5.0°.

3.3. Solution structure of the DNA-binding domain of AtTRB2

The secondary structure of AtTRB2$_{1-64}$ contains three α-helices (Helix 1, residues Pro10 to His23; Helix 2, Trp28 to Ser33; Helix 3, Asn46 to Val58) and connecting loops as those of other telomere binding proteins with a Myb domain (Fig. 2B–D). The helical Nuclear Overhauser Effect (NOEs) such as $d_{\alpha\beta}(i,i+3)$, $d_{\alpha N}(i,i+3)$, and $d_{\alpha N}(i,i+4)$ in ^{13}C-edited and ^{15}N-edited NOESY spectra manifested the helical conformation of these regions (Fig. 2B). The backbone atoms N, C_{α}, and C′ of the final 20 structures over the energy-minimized average structure was superimposed for residues 10 through 58 (Fig. 2C and D). For these residues holding the secondary structure, the average root-mean-square deviation (RMSD) values relative to the mean coordinates of 20 representative conformers were calculated to be 0.41 ± 0.08 Å for the backbone atoms and 1.03 ± 0.13 Å for the heavy atoms, respectively. The structural statistics are listed in Table 1. The dihedral angles Φ against Ψ of each amino acid residues in the final structures were adequately distributed in a Ramachandran plot. This result signified that the final structures have no steric collisions between atoms, and thermodynamically fold into well-defined structures. A salt bridge between Glu12 (in helix 1), Lys52 (in helix 3), and Arg44 (in turn 2) was detected (Fig. 3A). This relatively weak ionic interaction contributes to the stability of the folding structure as well as hydrophobic interaction. The residues Leu16, Val20, Trp28, Ile31, Leu32, Leu41, Leu49, Trp53, and Ile56 constituted a hydrophobic core and participated in maintaining

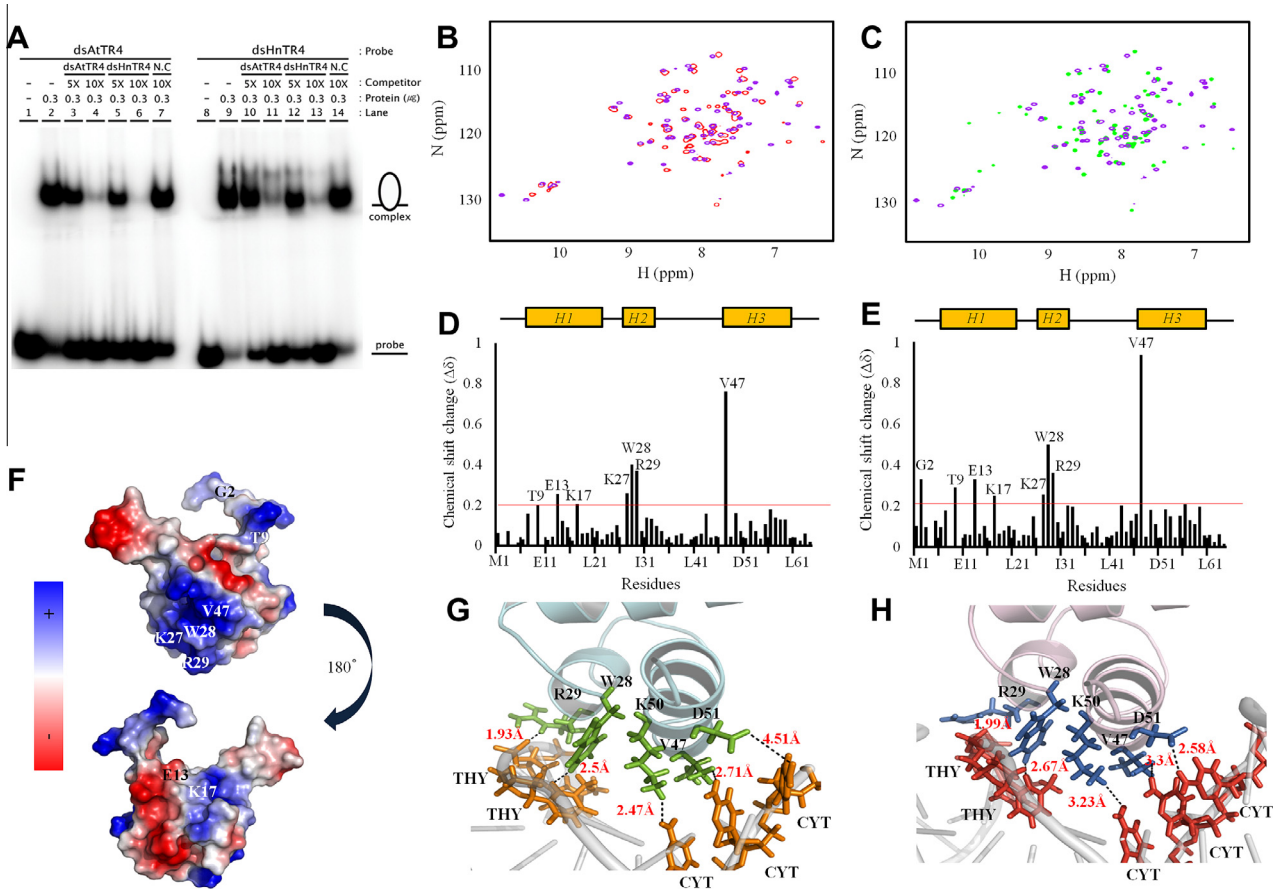

Fig. 4. NMR characterization of the interaction between AtTRB2$_{1-64}$ and telomeric DNAs. (A) Competitive EMSA assay demonstrated that AtTRB2 interacts with both plant (left panel) and human types (right panel) of telomeric DNA. (B, C) $^{1}H–^{15}N$ HSQC spectrum of AtTRB2$_{1-64}$ with plant telomeric DNA (B) and human telomeric DNA (C). Free state of AtTRB2$_{1-64}$ is colored purple. Plant and human telomeric DNA states are colored red and green, respectively. (D, E) Amide chemical shift perturbations of AtTRB2$_{1-64}$ upon binding to plant telomere (D) and human telomere (E). In each case, the average chemical shift changes were calculated using the formula $\Delta\delta_{total} = \{(\Delta\delta H^N)^2 + (0.17 \times \Delta\delta N^H)^2\}^{1/2}$, where $\Delta\delta H^N$ and $\Delta\delta N^H$ are the amide proton and amide nitrogen chemical shift differences, respectively. (F) Surface charge models represent that DNA binding site on AtTRB2$_{1-64}$ have positive charges. (G, H) Each AtTRB2$_{1-64}$ structure is aligned onto the plant telomeric DNA (TTTAGGG) derived from NgTRF1 (PDB ID: 2QHB) (G) and the human telomeric DNA (TTAGGG) derived from hTRF1 (PDB ID: 1W0T) (H). The AtTRB2$_{1-64}$/plant and human telomeric DNA complex structures was calculated by HADDOCK program. (For interpretation of the references to colour in this figure legend, the reader is referred to the web version of this article.)

the structural integrity and stabilization of the overall tertiary structure (Fig. 3B–F). The distribution of these hydrophobic amino acid residues in the Myb domain probably has an effect on determining the tertiary structure by forming the hydrophobic interactions between themselves and interrupting the hydrogen bonding structures between ambient water molecules. Assigned chemical shifts values and the atomic coordinates for the solution structure of AtTRB2$_{1-64}$ were deposited in the Biological Magnetic Resonance Bank (BMRB) and Protein Data Bank (PDB) under accession codes 17950 and 2LJN, respectively.

3.4. Molecular interaction between AtTRB2$_{1-64}$ and telomeric DNA

To confirm the DNA binding capacity and determine the DNA binding peculiarity of AtTRB2$_{1-64}$ *in vitro*, EMSA assay and NMR titration experiments were performed. In EMSA assay, AtTRB2$_{1-64}$ was shown to have a similar binding affinity in both plant and human type telomeric DNA, and the protein/DNA complex was well broken out in the presence of the competitor (Fig. 4A). In addition, the telomeric DNA repeat-binding site of AtTRB2$_{1-64}$ was characterized by collecting of the $^{1}H–^{15}N$ HSQC spectra perturbation by titrating plant or human telomeres. In both cases, upon binding to telomeric DNA, the chemical shift positions of the amide nitrogen and amide proton resonances for the bound AtTRB2$_{1-64}$ were altered due to protein/DNA complex formation. This result revealed that AtTRB2$_{1-64}$ could not only bind to plant telomere but also to human telomere, therefore AtTRB2 is regarded as a novel protein distinguished from other known plant telomere-binding proteins (Fig. 4B and C). Some residues that were perturbed by binding with a DNA molecule were detected, and from these results it is considered that Helix 2 and Helix 3 could be involved in DNA recognition. The largest chemical shift perturbations for both cases were observed for residues Trp28, Arg29 (in Helix 2), and Val47 (in Helix 3) (Fig. 4D and E). In particular, Arg29 of the Myb-like domain is a conserved residue only in the case of plant proteins and this positive residue may come into contact with DNA molecules directly. Because Helix 3 was located close to Helix 2 compared to other plant telomere-binding proteins and was packed with Helix 2, these helices could intercalate together into the major groove of human telomeric DNA with shorter sequences as well as plant telomeric DNA. The surface charge model shows that DNA binding sites on AtTRB2$_{1-64}$ have positive charges (Fig. 4F). Based on the NMR titration, the complex models of the AtTRB2$_{1-64}$ and telomeric DNA were constructed (Fig. 4G and H). The models were manufactured from the crystalline structures of the NgTRF1 (PDB ID: 2QHB) and hTRF1 (PDB ID: 1W0T) with DNA [15,36]. The DNA-binding domains in these complexes were replaced by AtTRB2$_{1-64}$. In two HSQC spectra for

titration, the patterns of resonance peaks corresponding to the binding mode were slightly different between the complexes with plant telomere and those with human telomere. This difference would provide a clue of biological evolution between plant and human species.

3.5. Structural comparison of AtTRB2$_{1-64}$ and the DNA-binding domain of other telomere-binding proteins

In the interest of structural comparison, structural relatedness in the three dimensional coordinates only was evaluated using the distance matrix alignment (DALI) method search [37,38]. The results matched up with a number of DNA-binding proteins with high *Z*-scores ($2.0 \leqslant Z\text{-score} \leqslant 6.7$). Specifically, human telomeric repeat binding factor 1 (hTRF1) in a protein/DNA complex state (PDB ID: 1IV6), possessed the highest structural homology to AtTRB2$_{1-64}$. Human TRF1 is composed of three helical regions (Trp385-Tyr398, Trp403-His409, and Ser417-Lys429) and two turns (Gly399-Asn402 and Tyr410-Thr416) [36]. Additionally, in the other structure known plant telomere-binding proteins, such as RTBP (PDB ID: 2ROH) in *Oryza sativa* or NgTRF1 (PDB ID: 2QHB) in *Nicotiana tabacum*, the additional fourth helix exists in the Myb-extension domain. This helix is crucial for stabilizing the overall structure by interacting with helix 1 and helix 3 comprehensively [39,15]. Furthermore, the forth helix is indispensable for the recognition of DNA sequences [39,15]. As compared with the telomere-binding domain in plants with AtTRB2$_{1-64}$, the overall topology of three helices was very similar. Also, compared to hTRF1 and hTRF2, helix 2 of AtTRB2$_{1-64}$ is shorter, and turn 2 connecting helix 2 to helix 3 is slightly longer than the coinciding region in hTRF1 (PDB ID: 1IV6) and hTRF2 (PDB ID: 1XG1). However, the overall configurations on the secondary structure of hTRF1, hTRF2, and AtTRB2$_{1-64}$ were about the same. In the structure, the backbone RMSD value between those structures was calculated to be 2.05 and 2.13 Å, respectively. Therefore, it was concluded that were it not for the Myb-extension domain in which the essential fourth helix subsists, similar to hTRF proteins [40,41], AtTRB2$_{1-64}$ does not only maintain the stability of the global structure, but also binds to double-stranded telomeric DNAs.

Acknowledgments

This work was supported by Mid-career Researcher Program (NRF-2013R1A2A2A01068963) and supported in part by Basic Science Research Program (No. NRF-2013 R1A12009383 to M.H.C.) through NRF grant funded by the MEST. J.H. Yun and W.K. Lee are recipients of Brain Korea 21 graduate student scholarship.

References

[1] M.N. Conrad, J.H. Wright, A.J. Wolf, V.A. Zakian, RAP1 protein interacts with yeast telomeres in vivo: overproduction alters telomere structure and decreases chromosome stability, Cell 63 (1990) 739–750.
[2] E.J. Richards, F.M. Ausubel, Isolation of a higher eukaryotic telomere from *Arabidopsis thaliana*, Cell 53 (1988) 127–136.
[3] K. Collins, Mammalian telomeres and telomerase, Curr. Opin. Cell Biol. 12 (2000) 378–383.
[4] J.W. Shay, S. Bacchetti, A survey of telomerase activity in human cancer, Eur. J. Cancer 33 (1997) 787–791.
[5] W.E. Wright, M.A. Piatyszek, W.E. Rainey, W. Byrd, J.W. Shay, Telomerase activity in human germline and embryonic tissues and cells, Dev. Genet. 18 (1996) 173–179.
[6] N.W. Kim, M.A. Piatyszek, K.R. Prowse, C.B. Harley, M.D. West, P.L. Ho, G.M. Coviello, W.E. Wright, S.L. Weinrich, J.W. Shay, Specific association of human telomerase activity with immortal cells and cancer, Science 266 (1994) 2011–2015.
[7] V. Lundblad, Molecular biology. Telomeres keep on rappin, Science 288 (2000) 2141–2142.
[8] C.I. Nugent, V. Lundblad, The telomerase reverse transcriptase: components and regulation, Genes Dev. 12 (1998) 1073–1085.
[9] C.W. Greider, Telomere length regulation, Annu. Rev. Biochem. 65 (1996) 337–365.
[10] D. Rhodes, L. Fairall, T. Simonsson, R. Court, L. Chapman, Telomere architecture, EMBO Rep. 3 (2002) 1139–1145.
[11] K. Ogata, S. Morikawa, H. Nakamura, A. Sekikawa, T. Inoue, H. Kanai, A. Sarai, S. Ishii, Y. Nishimura, Solution structure of a specific DNA complex of the Myb DNA-binding domain with cooperative recognition helices, Cell 79 (1994) 639–648.
[12] J. Tanikawa, T. Yasukawa, M. Enari, K. Ogata, Y. Nishimura, S. Ishii, A. Sarai, Recognition of specific DNA sequences by the c-myb protooncogene product: role of three repeat units in the DNA-binding domain, Proc. Natl. Acad. Sci. U.S.A. 90 (1993) 9320–9324.
[13] J.W. Dubendorff, L.J. Whittaker, J.T. Eltman, J.S. Lipsick, Carboxy-terminal elements of c-Myb negatively regulate transcriptional activation in cis and in trans, Genes Dev. 6 (1992) 2524–2535.
[14] E.Y. Yu, S.E. Kim, J.H. Kim, J.H. Ko, M.H. Cho, I.K. Chung, Sequence-specific DNA recognition by the Myb-like domain of plant telomeric protein RTBP1, J. Biol. Chem. 275 (2000) 24208–24214.
[15] S. Ko, S.H. Jun, H. Bae, J.S. Byun, W. Han, H. Park, S.W. Yang, S.Y. Park, Y.H. Jeon, C. Cheong, W.T. Kim, W. Lee, H.S. Cho, Structure of the DNA-binding domain of NgTRF1 reveals unique features of plant telomere-binding proteins, Nucleic Acids Res. 36 (2008) 2739–2755.
[16] C.M. Chen, C.T. Wang, C.H. Ho, A plant gene encoding a Myb-like protein that binds telomeric GGTTAG repeats in vitro, J. Biol. Chem. 276 (2001) 16511–16519.
[17] M.G. Hwang, K. Kim, W.K. Lee, M.H. Cho, AtTBP2 and AtTRP2 in Arabidopsis encode proteins that bind plant telomeric DNA and induce DNA bending in vitro, Mol. Genet. Genomics 273 (2005) 66–75.
[18] M.G. Hwang, I.K. Chung, B.G. Kang, M.H. Cho, Sequence-specific binding property of *Arabidopsis thaliana* telomeric DNA binding protein 1 (AtTBP1), FEBS Lett. 503 (2001) 35–40.
[19] M. Feldbrugge, M. Sprenger, K. Hahlbrock, B. Weisshaar, PcMYB1, a novel plant protein containing a DNA-binding domain with one MYB repeat, interacts in vivo with a light-regulatory promoter unit, Plant J. 11 (1997) 1079–1093.
[20] C.O. Marian, S.J. Bordoli, M. Goltz, R.A. Santarella, L.P. Jackson, O. Danilevskaya, M. Beckstette, R. Meeley, H.W. Bass, The maize Single myb histone 1 gene, Smh1, belongs to a novel gene family and encodes a protein that binds telomere DNA repeats in vitro, Plant Physiol. 133 (2003) 1336–1350.
[21] W.K. Lee, J.H. Yun, W. Lee, M.H. Cho, DNA-binding domain of AtTRB2 reveals unique features of a single Myb histone protein family that binds to both Arabidopsis- and human-type telomeric DNA sequences, Mol. Plant 5 (2012) 1406–1408.
[22] P. Schrumpfova, M. Kuchar, G. Mikova, L. Skrisovska, T. Kubicarova, J. Fajkus, Characterization of two *Arabidopsis thaliana* myb-like proteins showing affinity to telomeric DNA sequence, Genome 47 (2004) 316–324.
[23] G.W. Vuister, A. Bax, Quantitative J correlation: a new approach for measuring homonuclear three bond J(HNHa) coupling constants in 15N-enriched proteins, J. Am. Chem. Soc. 115 (1993) 7772–7777.
[24] S. Grzesiek, A. Bax, Improved 3D triple-resonance NMR techniques applied to a 31-kDa protein, J. Magn. Reson. 96 (1992) 432–440.
[25] D.R. Muhandiram, L.E. Kay, Gradient-enhanced triple-resonance three-dimensional NMR experiments with improved sensitivity, J. Magn. Reson. 103 (1994) 203–216.
[26] M. Ikura, L.E. Kay, A. Bax, A novel approach for sequential assignment of ^{1}H, ^{13}C, and ^{15}N spectra of proteins: heteronuclear triple-resonance three-dimensional NMR spectroscopy. Application to calmodulin, Biochemistry 29 (1990) 4659–4667.
[27] M. Piotto, V. Saudek, V. Sklenar, Gradient-tailored excitation for single-quantum NMR spectroscopy of aqueous solutions, FEBS Lett. 2 (1992) 661–665.
[28] A.L. Davis, J. Keeler, E.D. Laue, D. Moskau, Experiments for recording pure absorption heteronuclear correlation spectra using pulsed field gradients, J. Magn. Reson. 98 (1992) 207–216.
[29] F. Delaglio, S. Grzesiek, G.W. Vuister, G. Zhu, J. Pfeifer, A. Bax, NMRPipe: a multidimensional spectral processing system based on UNIX pipes, J. Biomol. NMR 6 (1995) 277–293.
[30] T.D. Goddard, D.G. Kneller, SPARKY 3, University of California, San Francisco, CA, 2004.
[31] G. Cornilescu, F. Delaglio, A. Bax, Protein backbone angle restraints from searching a database for chemical shift and sequence homology, J. Biomol. NMR 13 (1999) 289–302.
[32] T. Herrmann, P. Guntert, K. Wuthrich, Protein NMR structure determination with automated NOE assignment using the new software CANDID and he torsion angle dynamics algorithm DYANA, J. Mol. Biol. 319 (2002) 209–227.
[33] R.A. Laskowski, J.A. Rullmannn, M.W. MacArthur, R. Kaptein, J.M. Thornton, AQUA and PROCHECK-NMR: programs for checking the quality of protein structures solved by NMR, J. Biomol. NMR 8 (1996) 477–486.
[34] R. Koradi, M. Billeter, K. Wuthrich, MOLMOL: a program for display and analysis of macromolecular structures, J. Mol. Graph. 14 (51–55) (1996) 29–32.
[35] W.L. DeLano, The PyMOL Molecular Graphics System, DeLano Scientific, San Carlos, CA, 2002.

[36] T. Nishikawa, H. Okamura, A. Nagadoi, P. Konig, D. Rhodes, Y. Nishimura, Solution structure of a telomeric DNA complex of human TRF1, Structure 9 (2001) 1237–1251.
[37] L. Holm, C. Sander, Dali: a network tool for protein structure comparison, Trends Biochem. Sci. 20 (1995) 478–480.
[38] L. Holm, C. Sander, Alignment of three-dimensional protein structures: network server for database searching, Methods Enzymol. 266 (1996) 653–662.
[39] S.C. Sue, H.H. Hsiao, B.C. Chung, Y.H. Cheng, K.L. Hsueh, C.M. Chen, C.H. Ho, T.H. Huang, Solution structure of the *Arabidopsis thaliana* telomeric repeat-binding protein DNA binding domain: a new fold with an additional C-terminal helix, J. Mol. Biol. 356 (2006) 72–85.
[40] R. Court, L. Chapman, L. Fairall, D. Rhodes, How the human telomeric proteins TRF1 and TRF2 recognize telomeric DNA: a view from high-resolution crystal structures, EMBO Rep. 6 (2005) 39–45.
[41] S. Hanaoka, A. Nagadoi, Y. Nishimura, Comparison between TRF2 and TRF1 of their telomeric DNA-bound structures and DNA-binding activities, Protein Sci. 14 (2005) 119–130.